Sheffield Hallam University

# Recent progress in magnesium-based thermoelectric materials

SANTOS, Rafael, AMINORROAYA YAMINI, Sima <http://orcid.org/0000-0002-2312-8272> and DOU, Shi Xue

Available from Sheffield Hallam University Research Archive (SHURA) at:

https://shura.shu.ac.uk/18567/

This document is the Accepted Version [AM]

**Citation:**

SANTOS, Rafael, AMINORROAYA YAMINI, Sima and DOU, Shi Xue (2018). Recent progress in magnesium-based thermoelectric materials. Journal of Materials Chemistry A, 6 (8), 3328-3341. [Article]

**Copyright and re-use policy**

See http://shura.shu.ac.uk/information.html

**Sheffield Hallam University Research Archive**
http://shura.shu.ac.uk

Please do not adjust margins

Journal of Materials Chemistry A

REVIEW

# Recent progress in magnesium-based thermoelectric materials

Rafael Santos,[a] Sima Aminorroaya Yamini[a,b]* and Shi Xue Dou[a]

Click or tap here to enter text.Received 00th January 20xx, Accepted 00th January 20xx

DOI: 10.1039/x0xx00000x

www.rsc.org/

Magnesium-based thermoelectric materials ($Mg_2X$, $X$ = Si, Ge, Sn) are considered one of the most attractive groups for large-scale application, due to their materials' high availability, low cost, low mass density, and reasonably high efficiency. In this work, we present an overview of the recent developments relating to magnesium-based thermoelectric materials and review the current approaches towards high thermoelectric efficiency.

## 1. Introduction

The combined waste energy in electricity generation and transportation, only in the USA, represents 80.0 percent of the total losses as these industries are the most energy inefficient[1]. Furthermore, the majority of the rejected energy is in the form of waste heat[2] which has prompted electricity generation[3, 4], transportation[5, 6] and other heavy industries such as metal processing[7, 8] to consider waste heat recovery technologies such as thermoelectric generation. Solid-state thermoelectric devices directly convert heat to electricity. Although traditional dynamic heat recovery technologies are more efficient, particularly in large-scale applications, thermoelectric technology shows promising advantages due to its having no moving parts, virtually eliminating the need for maintenance, as well as long life and reliability, silent operation, and high scalability[9].

The applicability of thermoelectric devices is highly dependent on the materials used in their fabrication. Higher efficiency devices based on bismuth or tellurium are usually not economically feasible[10, 11], some industries are eliminating the use of toxic elements such as lead[12], and automotive applications have weight related restrictions, requiring low density materials[11, 13]. Magnesium-based thermoelectric materials possess the right characteristics to address these challenges while exhibiting high conversion efficiencies in the medium-to-high temperature range (250 to 650 °C), making them the target of great research interest.

Here, we summarise recent developments in magnesium-based thermoelectric materials, review the strategies used to obtain high efficiencies, and describe their associated mechanisms, while comparing the different synthesis techniques employed.

### 1.1 Thermoelectric efficiency

The main focus in thermoelectrics research has been driven by the pursuit of higher thermoelectric conversion efficiencies, defined by the dimensionless thermoelectric material figure-of-merit $zT$,

$$zT = \frac{S^2\sigma}{\kappa_{tot}}T \qquad (1)$$

where $S$ is the Seebeck coefficient, $\sigma$ the electrical conductivity, $\kappa_{tot}$ the total thermal conductivity and $T$ the absolute temperature. The $zT$ is dependent on the doping level of the material[14], making optimization of the charge carrier concentration essential for obtaining a fair comparison between different thermoelectric materials. Furthermore, the thermoelectric figure-of-merit $zT$ is a function of $S$, $\sigma$ and $\kappa$, which share dependencies on many fundamental thermoelectric properties, such as the charge carrier concentration[15]. Balancing the effects of these overlapping dependencies creates significant challenges when selecting the correct strategy towards higher $zT$.

The thermoelectric quality factor, $B$[14], summarizes the most important characteristics that a thermoelectric material should exhibit in order to achieve the maximum $zT$:

$$B = \frac{2k_B^2\hbar}{3\pi}\frac{N_V C_l}{m_I^{*}\Xi^2\kappa_{lat}} \qquad (2)$$

where $k_B$ is the Boltzmann constant, $\hbar$ the reduced Planck constant, $N_V$ the valley degeneracy, $C_l$ the average longitudinal elastic modulus, $m_I^*$ the inertial effective mass, $\Xi$ the deformation potential coefficient, $\kappa_{lat}$ the lattice component of the thermal conductivity, and $T$ the absolute temperature. The $B$ factor itself also has some limitations, as it operates on the assumption that changing the charge carrier concentration merely affects the Fermi level, without any significant impact on scattering or on the electronic structure[14]. The inertial effective mass $m_I^*$ is defined differently from the effective mass $m^*$, which is used for semiconductors whose band

[a] Australian Institute of Innovative Materials (AIIM), Innovation Campus, University of Wollongong, NSW, 2500, Australia.
[b] Department of Engineering and Mathematics, Sheffield Hallam University, Sheffield, S1 1WB, United Kingdom.

† Footnotes relating to the title and/or authors should appear here.
Electronic Supplementary Information (ESI) available: [details of any supplementary information available should be included here]. See DOI: 10.1039/x0xx00000x



Please do not adjust margins

Please do not adjust margins



structures can be described by a single parabolic band model, where the conduction band minimum and the valence band maximum are positioned at the centre of the Brillouin Zone (crystal momentum $k = 0$). Many thermoelectric materials have several conduction band minima and valence band maxima at different positions in the Brillouin Zone, creating degenerated valleys ($N_V$). In this case, the total density of states (DOS) effective mass is defined as $m_d^*$ [16], where:

$$m_d^* = N_V^{2/3} m_b^* \quad (3)$$

and $m_b^*$ is the DOS effective mass of a single valley[17]. $m_I^*$ can be seen as the weighted average effective mass of valleys in semiconductors with anisotropic band structures, and is used to calculate the electrical conductivity. Generally, an increase in $m_I^*$ results in an increase in $m_b^*$. Defining the effective masses in this way is essential to understanding the thermoelectric quality factor, as increases in $m_d^*$ usually lead to improvements in the Seebeck coefficient. According to Equation 3, this can be achieved either through a higher $N_V$ or a large $m_b^*$. The latter also means an increased $m_I^*$, however, which is detrimental to $B$ (Equation 2), while a higher $N_V$ leads to a higher thermoelectric quality factor[17-19]. This is also verified if the thermoelectric figure-of-merit is considered, as a higher $m_I^*$ leads to a lower electrical conductivity and $zT$. Moreover, the thermoelectric quality factor indicates that a low lattice thermal conductivity $\kappa_{lat}$ should result in higher thermoelectric performance. This conclusion is commonly pursued in thermoelectric materials research, and specifically in magnesium-based thermoelectric materials, by promoting phonon-scattering through point defects in alloys[9, 20], secondary phases[21-24], or pores[25], which generate additional boundaries, further contributing to the scattering of phonons and consequently to the reduction of the lattice thermal conductivity. The strategies currently used to depress the lattice thermal conductivity of magnesium-based thermoelectric materials are discussed in more detail later in this review.

The present market and safety regulations have steered the research and development of thermoelectric materials towards lead-free, environmentally friendly, and cheap materials[26] made from abundant elements. Magnesium-based alloys are viewed as potential replacements for the heavily studied PbTe and others[27-29], due to their non-toxicity, high power factor (PF), and low mass density[30, 31].

Thermoelectric materials based on $Bi_2Te_3$, PbTe, $CoSb_3$, and GeTe compounds remain the most interesting materials for potential applications due to their high thermoelectric performances (Table 1). Figure 1 compares the $zT$ values of the current best performing medium-to-high temperature thermoelectric materials, highlighting the place of magnesium-based thermoelectric materials.

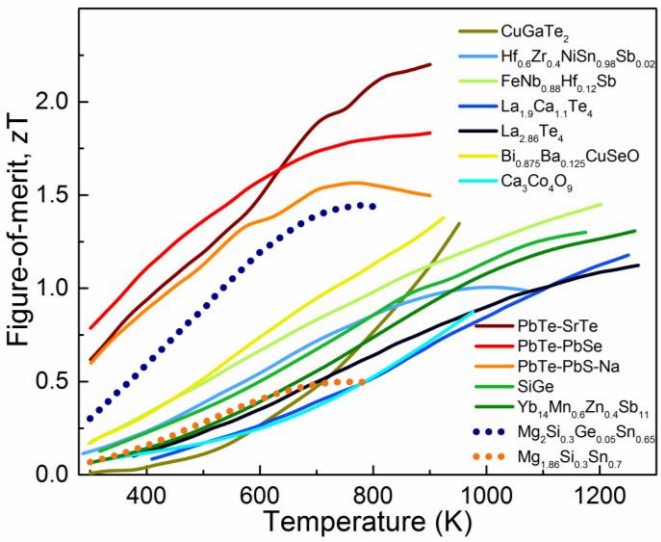


Figure 1. State-of-art $zT$ for medium-to-high temperature thermoelectric materials. $Mg_2Si_{0.3}Ge_{0.05}Sn_{0.65}$ was obtained from [32] and $Mg_{1.86}Si_{0.3}Sn_{0.7}$ from [43], while the rest of the data was compiled from [44].

## 2. Magnesium-based thermoelectric materials

$Mg_2X$ ($X$ = Si, Ge, Sn) materials are intermetallic alloys that have been studied for decades[38, 39] as potential high $zT$ thermoelectric materials. The application of these materials in thermoelectric generators for the automotive industry, for example, requires other characteristics beyond thermoelectric performance such as plastic deformation and high fracture toughness in order to survive mechanical stress due to vibrations and temperature cycling[40]. The automotive industry, in particular, requires these generators to be as light as possible, and low mass density materials such as magnesium-based thermoelectrics, with density of ~ 2 g/cm$^3$, have the advantage over the more common PbTe, $CoSb_3$, or $Bi_2Te_3$ with densities between 6.5 and 8.5 g/cm$^3$. The binary compounds of the $Mg_2$(Si, Ge, Sn) system – $Mg_2Si$, $Mg_2Ge$, and $Mg_2Sn$ – are known to have high thermal conductivity[41, 42] (Table 2), which is reduced by alloying[42] (Table 1), making this class of compounds one of main approaches towards high $zT$.

Table 1. Thermoelectric properties of state-of-art thermoelectric materials.

| Material | $zT$ | $S$ $\mu V/K$ | $\sigma$ $(\Omega \cdot m)^{-1}$ | $\kappa_{tot}$ $W/mK$ | $\kappa_{lat}$ $W/mK$ | $T$ $K$ | Ref. |
|---|---|---|---|---|---|---|---|
| $Mg_{2.16}(Si_{0.3}Ge_{0.05}Sn_{0.65})_{0.98}Sb_{0.02}$ | 1.45 | -215 | $9.5\times10^4$ | 2.35 | 1.15 | 750 | 32 |
| $Bi_{0.5}Sb_{1.5}Te_3$ | 1.86 | 242 | $6.5\times10^4$ | 0.65 | 0.32 | 320 | 33 |
| $(PbTe)_{0.8}(PbS)_{0.2}$ | 2.30 | 240 | $3.5\times10^4$ | 0.82 | 0.35 | 923 | 34 |
| $Co_4Sb_{11.5}Te_{0.5}$ | 1.15 | -200 | $1.3\times10^5$ | 3.50 | 1.50 | 880 | 35 |
| $Ge_{0.87}Pb_{0.13}Te$ | 2.20 | 195 | $1.0\times10^5$ | 2.20 | 1.20 | 718 | 36 |
| $Si_{80}Ge_{20}$ | 1.50 | -290 | $3.5\times10^4$ | 2.30 | 1.38 | 1173 | 37 |


This journal is © The Royal Society of Chemistry 2017

Please do not adjust margins

Please do not adjust margins



Table 2. Summary of electronic and physical properties of Mg-based binary alloys[41, 42].

| | $Mg_2Si$ | $Mg_2Ge$ | $Mg_2Sn$ |
|---|---|---|---|
| $a$ (Å) | 6.338 | 6.385 | 6.765 |
| Density (g/cm$^3$) | 1.88 | 3.08 | 3.59 |
| $E_g$ at 0 K (eV) | 0.77 | 0.74 | 0.35 |
| $dE_g/dT$ at 0 K (eV/K) | $-6\times10^{-4}$ | $-8\times10^{-4}$ | $-3.2\times10^{-4}$ |
| $\Delta E$ at 0 K (eV) | 0.4 | 0.58 | 0.16 |
| $\kappa_L$ (W/mK) | 7.9 | 6.6 | 5.9 |
| Melting point (K) | 1375 | 1388 | 1051 |

All $Mg_2X$ ($X$ = Si, Ge, Sn) compounds adopt the face-centered cubic (FCC) crystal structure, and their structural symmetry corresponds to the *Fm*-3*m* space group (#225)[48]. The unit cell is composed of 12 atoms, with the $X^{4-}$ ions occupying the four face-centered cubic positions and the $Mg^{2+}$ ions the eight centered tetrahedral sites (Figure 2a). These compounds have very similar band structures, with the valence band maximum (VBM) at the Γ point in the Brillouin zone (Figure 2b) and the conduction band minimum (CBM) at X, resulting in an indirect energy gap ($E_g$)[47]. The CBM is characterized as having a split band, where the light ($C_L$) and heavy ($C_H$) bands are separated by an energy offset ($\Delta E$)[42]. This split conduction band is the focus of many studies due to its considerable influence on the electrical properties of these compounds[28, 41, 49].

The highest reported $zT$ values for binary, ternary, and quaternary *n*- and *p*-type Mg-based thermoelectric alloys are shown in Figure 3. Most studies have explored *n*-type materials, resulting in a maximum $zT$ of 1.45 at 775 K (502 °C), while for *p*-type Mg-based thermoelectrics, the maximum $zT$ achieved is 0.5 at 700 K (427 °C). Despite the popularity of these materials, particularly for future applications in thermoelectric devices, there is limited information available on their thermal stability and mechanical properties. Table 3 summarizes the relevant mechanical properties of magnesium-based thermoelectric materials.

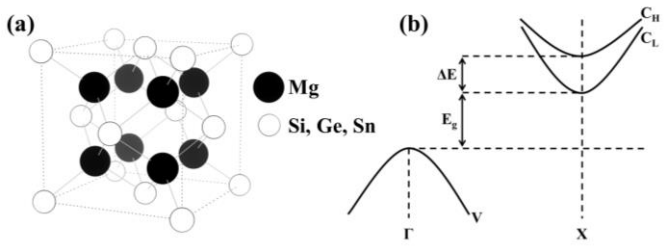


Figure 2. (a) Crystal structure and (b) simplified band structure of $Mg_2X$ ($X$ = Si, Ge, Sn) alloys. $C_H$, $C_L$, and $V$ represent the heavy conduction band, light conduction band, and valence band, respectively[15, 47].

Table 3. Mechanical properties of Mg-based thermoelectric materials at room temperature. $E$ is the Young's modulus, $G$ the sheer modulus, $H$ the Vickers hardness, $\alpha_L$ is the linear coefficient of thermal expansion, and $v$ the Poisson's ratio. References a and b are [45] and [46], respectively.

| Composition | $E$ GPa | $G$ GPa | $H$ GPa | $\alpha_L$ $10^{-6}$/K | $v$ |
|---|---|---|---|---|---|
| $Mg_2Si$ | 117.3[a] | 49.5[a] | 5.3[a] | 16[b] | 0.185[a] |
| $Mg_2Ge$ | 105.6[b] | 45.0[b] | - | 15[b] | 0.173[b] |
| $Mg_2Sn$ | 80.3[a] | 34.2[a] | 1.2[a] | 19[b] | 0.176[a] |
| $Mg_{2.08}Si_{0.4}Sn_{0.6}$ | 88.1[a] | 36.9[a] | 3.1[a] | 20[a] | 0.195[a] |

## 3. Strategies to improve the $zT$ of Mg-based thermoelectric materials

### 3.1 Alloying

Early research on magnesium-based thermoelectric materials was dedicated to the study of the binary phases – $Mg_2Si$, $Mg_2Ge$ and $Mg_2Sn$ – and their properties. The main leaps in the performance of these materials were obtained, however,

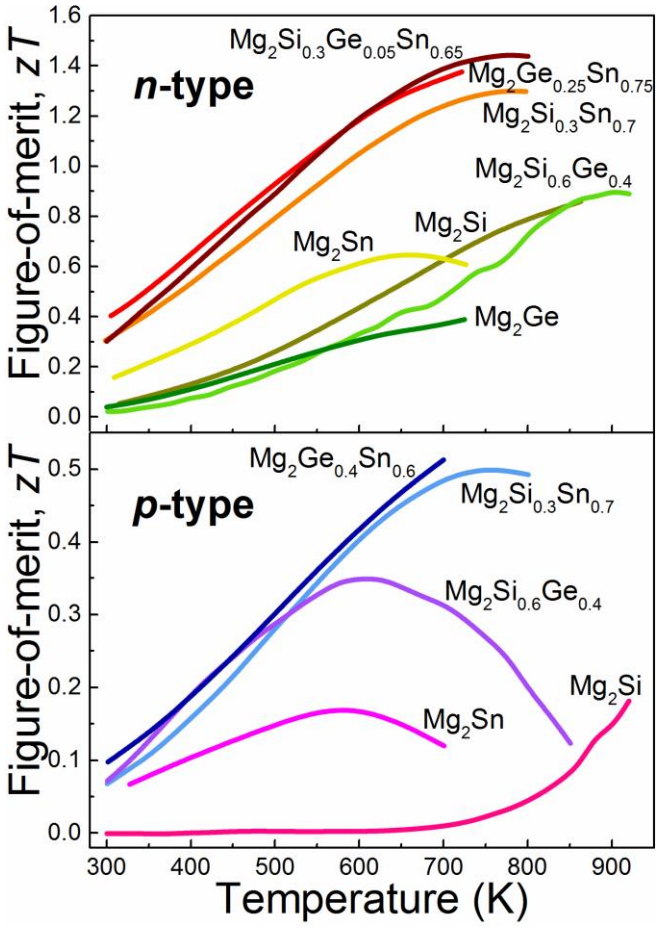


Figure 3. Overview of the highest reported $zT$ values for Mg-based thermoelectric materials. (a) *n*–type: $Mg_2Si$[50], $Mg_2Ge$[28], $Mg_2Sn$[28], $Mg_2Si_{0.6}Ge_{0.4}$[51], $Mg_2Si_{0.3}Sn_{0.7}$[52], $Mg_2Ge_{0.25}Sn_{0.75}$[53], $Mg_2Si_{0.3}Ge_{0.05}Sn_{0.65}$[32]. (b) *p*-type: $Mg_2Si$[51], $Mg_2Sn$[54], $Mg_2Si_{0.6}Ge_{0.4}$[55], $Mg_2Si_{0.3}Sn_{0.7}$[43], $Mg_2Ge_{0.4}Sn_{0.6}$[56].



Please do not adjust margins

Please do not adjust margins



by studying the atomic substitution of one element by one or more elements, which is known as alloying. The main purpose of alloying in thermoelectrics research is the creation of point defects through solid solution alloying, which consists of point substitutions using isoelectronic elements. The crystal structure is maintained, while the increased atomic mass contrast increases phonon scattering[9, 20] leading to lower lattice thermal conductivity. At higher concentrations of the substituting element, alloying can have effects beyond creating point defects. The presence of atoms with different characteristics leads to the straining of the crystal structure, which can have a significant influence on the electronic characteristics due to increased electron scattering and consequently, lower charge carrier mobility. These changes in the crystal structure, even if minimal, can have a substantial impact on the electronic band structure – with positive or negative consequences for the thermoelectric efficiency due to changes to the electronic band gap and the relative positions of multiple bands[57]. The latter effect has been the main motivation behind the study of Mg-based alloys, by exploiting the convergence of the two lowest conduction bands, leading to a greater power factor, or by increasing the band gap, which suppresses the detrimental impact of the bipolar effect[20, 57].

### 3.2 Solid solutions

The solid solutions of $Mg_2X$ ($X$ = Si, Ge, Sn) pseudo-binary compounds – $Mg_2Si_{1-x}Sn_x$, $Mg_2Si_{1-x}Ge_x$, and $Mg_2Ge_{1-x}Sn_x$ – have been the subject of great interest due to the significant effect alloying has on their lattice thermal conductivity. Mass-difference scattering is the main mechanism responsible for the decreased lattice thermal conductivity when alloying, and therefore, it is no surprise that the $Mg_2Si_{1-x}Sn_x$ system exhibits the lowest $\kappa_{lat}$[58, 59] (Figure 4), as the atomic masses of Si, Ge, and Sn atoms are 28.1, 72.6, and 118.71 amu, respectively. For this reason, the $Mg_2Si$-$Mg_2Sn$ pseudo-binaries are considered the most interesting compounds for thermoelectric applications in the $Mg_2X$ system[59].

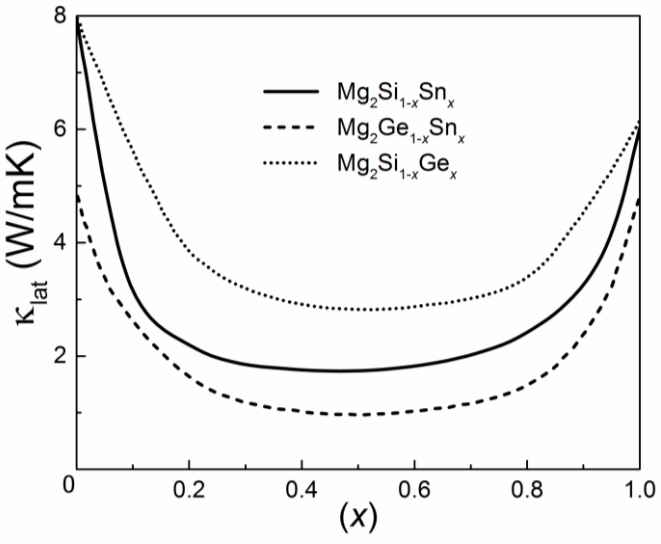


Figure 4. Lattice thermal conductivity as a function of composition of magnesium-based ternary alloys. Adapted from[58].

Alloying $Mg_2Si_{0.6}Sn_{0.4}$ with small amounts of Ge was demonstrated[60] to have a significant impact on the thermal conductivity of the matrix. The compound without Ge already exhibited nanosized phase-separated structures, and the addition of Ge led to the formation of more Ge-containing secondary phases, products of the reactions of Ge with Mg, Si, and Sn. These features were also refined with increased added Ge, which, along with the increased atomic mass difference due to Si substitution by Ge, led to lower lattice thermal conductivity at low Ge concentrations. The solid solutions of these compounds have naturally formed nanoscale features that contribute to the further scattering of phonons[60] (Figure 5b). Despite reports on the formation of complete solid solutions of compounds such as $Mg_2Si_{0.5}Sn_{0.5}$[61], thought to fall within the miscibility gap of $Mg_2Si$-$Mg_2Sn$, many studies report the observation of Si- and Sn-rich phases[60, 62, 63]. The morphology and size of these secondary phases depend mostly on the synthesis and processing techniques, which can be tuned to induce the formation of phonon-scattering features such as nanoprecipitates located within the matrix and/or at the grain boundaries[62, 64], or distortions in the lattice[62]. Sb-doped $Mg_2Si_{0.5}Sn_{0.5}$ prepared using spark plasma sintering (SPS) without the application of mechanical pressure resulted in samples with 37% porosity that exhibit a lattice thermal conductivity as low as 0.486 W/mK at 573 K[25] (Figure 5g), achieving a $zT$ of 1.63 at 615 K.

### 3.3 Nanostructuring

While alloying is an effective approach towards reducing the lattice thermal conductivity, the main mechanism through which it operates is the atomic mass contrast. The need to further reduce the lattice thermal conductivity led to the development of a collection of structural modifications at the nanoscale level commonly known as nanostructuring. This approach includes reduction of the grain size,[58, 65] and nanoprecipitates[23, 24] (Figure 5a) and nanoinclusions[63] (Figure 5c), with the intent of generating features with similar dimensions to the wavelength of phonons, thus scattering them. Obtaining nanosized crystalline matrices requires two main approaches: reduction of the grain size of the starting materials and control of the grain growth during synthesis/processing.[57]

#### 3.3.1 Grain size reduction

Theoretical studies on $Mg_2Si$ suggest that a 40% reduction in the lattice thermal conductivity can be obtained with a grain size of 20 nm due to the formation of phonon-scattering grain boundaries, although these would also scatter electrons and significantly decrease the electron mobility by 20%[66]. Powder processing techniques such as grinding and ball milling are commonly used techniques to process Mg-based thermoelectrics. Nonetheless, these present challenges, as

 This journal is © The Royal Society of Chemistry 2017

Please do not adjust margins

Please do not adjust margins



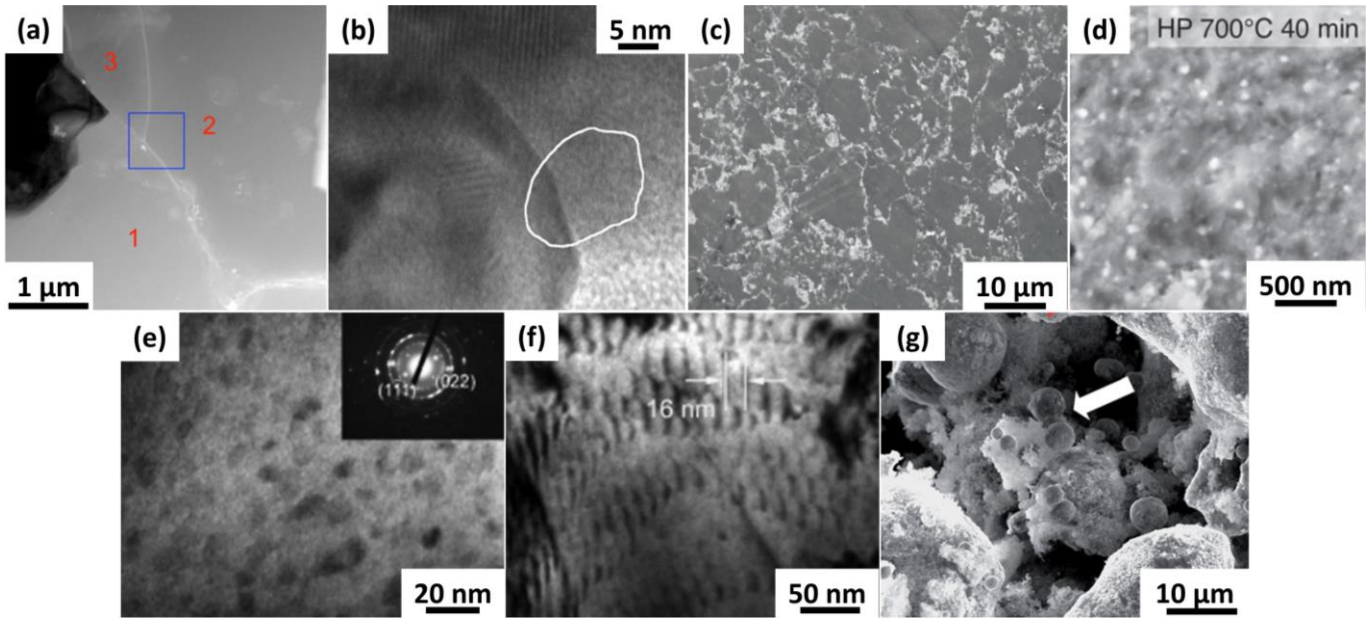


Figure 5. Examples of nanostructures in magnesium-based thermoelectric materials: (a) embedded SiC nanoparticles in the grain boundaries of $Mg_2Si_{0.7}Ge_{0.3}$ (bright particle close to the grain boundaries, inside the blue square)[24], (b) Sn/Ge-rich nanocrystallite in $Mg_2Si_{0.53}Sn_{0.4}Ge_{0.05}$[60], (c) $Mg_2Si$ grains coated with $Mg_2Sn$-rich nanolayers[63], (d) nanoprecipitates formed during annealing in $Mg_2Si$ matrix[67], (e) in-situ-formed 10 nm-sized nanodots in $Mg_2Si_{0.3925}Sn_{0.6}Sb_{0.0075}$ matrix[62], (f) nanoscale structural modulation, 16 nm in size, in $Mg_2Si_{0.3925}Sn_{0.6}Sb_{0.0075}$ matrix[62], (g) porous $Mg_2Si_{0.5}Sn_{0.5}$[25].

magnesium particles tend to agglomerate instead of fracturing due to their high ductility[53, 68], conveying the need to react the materials first, forming brittle $Mg_2X$ ($X$ = Si, Ge, Sn) compounds that can be easily milled to fine powders[53]. The detrimental scattering of electrons by grain boundaries is not reported as a significant effect in $Mg_2Si_{1-x}Sn_x$ solid solutions, and grain size reduction is seen as a pathway towards improving $zT$[62, 69] (Figure 5e and f).

#### 3.3.2 Addition of nanoparticles

The presence of nanosized features such as nanoprecipitates can be obtained through in-situ formation[62, 67] (Figure 5d) or by the introduction of nanoparticles at some point during the synthesis. The addition of silicon carbide (SiC) nanoparticles to $Mg_2Si_{0.676}Ge_{0.3}Bi_{0.024}$ has been recently reported[24] (Figure 5a), leading to increased $zT$. These nanoparticles have a significant impact on the thermal conductivity, despite the high thermal conductivity of SiC, lowering it to 1.82 W/mK at 773 K from 3.1 W/mK for Bi-doped $Mg_2Si$, resulting in a small increase in $zT$ despite the detection of a decrease in the electrical conductivity due to a detrimental effect on the electron mobility. The effect of $TiO_2$ nanoparticles in undoped $Mg_2Si$ was also reported to increase the $zT$, although no significant effect on the thermal conductivity was observed[70]. The authors reported a tenfold increase in the charge carrier concentration due to electrons donated by titanium atoms via a reaction of $TiO_2$ during sintering.

### 3.4 Band engineering

#### 3.4.1 Band convergence

Several works were recently dedicated to the study of the band structure of $Mg_2X$ ($X$ = Si, Ge, Sn) compounds[27, 42, 49, 71-75], focusing mostly on alloys with potential convergence of the two lowest conduction bands. The most interesting compositions are around $Mg_2Si_{1-x}Sn_x$ for $x$ = 0.60 – 0.70 [42, 49, 71, 76], where the conduction band convergence of the bottom conduction bands ($C_H$ and $C_L$) is reported to occur (Figure 6), along with increased band degeneracy ($N_V$). The origins of the increased $N_V$ are suggested to be owing to two main factors[27]: (i) at $x$ ~ 0.75, the Sn 4d states contribute by hybridizing with the Mg 3s states in the conduction band; (ii) the alloy-induced strain in the crystal lattice significantly affects the positions of the $C_H$ and $C_L$ bands, due to the consequent variation in the lattice parameters.

When the energy difference between the two bottom

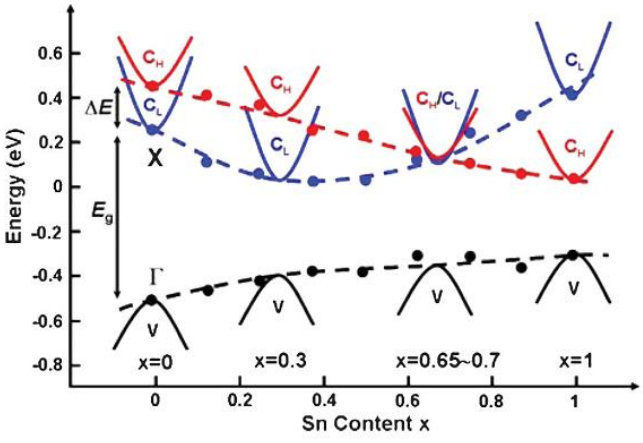


Figure 6. Relative position (in energy) of the two lowest conduction bands and the highest valence band as function of the Sn content in $Mg_2Si_{1-x}Sn_x$[49].



Please do not adjust margins

Please do not adjust margins



conductions bands is smaller than $2k_BT$, $N_V$ increases, leading to a higher carrier effective mass (Equation 3), which is reported to enhance the Seebeck coefficient[77] (Equation 4) without decreasing the charge carrier mobility ($\mu$) and, consequently, the electrical conductivity ($\sigma$, $\sigma = ne\mu$)[42, 49].

$$S = \frac{2k_B^2 T}{3e\hbar^2}\left(\frac{\pi}{3n}\right)^{\frac{2}{3}} m^*(1+r) \qquad (4)$$

where $k_B$ is the Boltzmann constant, $e$ the electron charge, $\hbar$ is the reduced Planck constant, $m^*$ the density of states effective mass, and $r$ the scattering parameter. Figure 6 shows the positions of the light and heavy conduction bands in relation to each other as a function of Sn content in $Mg_2Si_{1-x}Sn_x$. The composition at which the convergence of the conduction bands occurs corresponds to the Mg-based thermoelectrics reported to have the highest $zT$ – for $x$ = 0.65 – 0.70 – such as $Mg_2Si_{0.3}Ge_{0.05}Sn_{0.65}$[32] and $Mg_2Si_{0.3}Sn_{0.7}$[78] (Figure 3).

### 3.4.2 Doping

The charge carrier concentration governs the electronic characteristics of a thermoelectric material by having a direct influence on the electrical conductivity and the Seebeck coefficient through the positioning of the Fermi level in the band gap. Beyond that, the number of available carriers and the ratio between the electrons and holes play essential roles in these parameters, especially at higher temperature due to the bipolar effect[79]. Therefore, the primary step towards a higher $zT$ is through optimization of the charge carrier concentration, obtained through the doping of the matrix with a donor or acceptor element[9].

Numerous theoretical and experimental studies have reported on potential elemental dopants for $n$- and $p$-type $Mg_2X$ ($X$ = Si, Ge, Sn) thermoelectrics. The most commonly used $n$-type dopants are Bi[81, 84-86] and Sb[42, 52, 62, 84, 87, 88]. Both contribute one electron per substitution[84, 87] and are expected to occupy the $X$ site in $Mg_2X$ when $X$ = Si[84], Ge[85], or Sn[86]. As shown in Figure 3, $p$-type doping of these materials has not been as successful, although the number of dedicated studies on the synthesis of these materials is still limited. The most successful method for improving the $zT$ in magnesium-based thermoelectric materials has been inducing the convergence of the two conduction bands closest to the band gap, which has a profound effect on the $n$-type properties of these materials. The lack of a similar structure for the valence band limits the pathways available for achieving high performance.

Theoretical calculations have shown that the optimal charge carrier concentrations for $p$-type and $n$-type $Mg_2Si$ to achieve the same $zT$ at 850 K are $5.3 \times 10^{19}$ $cm^{-3}$ and $3.7 \times 10^{20}$ $cm^{-3}$, respectively[89]. This further constrains the avenues through which improvement is possible, as higher charge carrier concentrations require larger additions of $p$-type dopants, which need to be considered with respect to limits of solubility. Some of these dopants have already been identified, however, with Ag[51, 54], Li[43], and Ga[55] being the most commonly reported hole donors, which are expected to occupy the Mg site in the crystal structure[84-86]. Table 4 lists elemental dopants used in magnesium-based thermoelectric materials.

#### *Resonant states*

Generally, the charge carrier (or carriers) donated by the dopant element occupies energy levels within the band gap of the host phase, defining the Fermi level ($E_F$). In the case of $n$-type dopants as an example, a loosely bound electron is available to populate the conduction band, when excited with the amount of energy required to bridge the small gap. Some dopants, however, create resonant levels which contain charge carriers that fall inside the band, with the same energy as already occupied states. These interact, resonate, and create new energy states that will then resonate with other already present energy states, repeating the process several times. These interactions lead to a DOS distortion of the band (Figure 7), increasing the carrier effective mass without changing the carrier concentration, resulting in an increased Seebeck coefficient (Equation 4) and power factor (i.e. without a significant impact on $\sigma$).[2, 90]

Despite the impact that resonant states can have on the efficiency of thermoelectric materials, there are limited reports on doping Mg-based thermoelectrics with impurities that are expected to induce the formation of resonant states within the electronic bands. An exception to this is a work on first-principles calculations of the electronic band structure of $Mg_2Si$ and possible dopants, which suggests that Ni could potentially form resonant states within the conduction band, and Zn and Cd within the valence band[91].

Table 4. List of dopants used successfully in magnesium-based thermoelectric materials and respective thermoelectric characteristics, with some literature reports on the doping influence of non-stoichiometric interstitial magnesium.

| Composition | Dopant | Type | Max $n/p$ $10^{-20}$ $cm^{-3}$ | $zT$ | $T$ K | $S$ $\mu V/K$ | $\sigma$ $10^4$ $\Omega \cdot m$ | $\kappa_{tot}$ $W/mK$ | Ref. |
|---|---|---|---|---|---|---|---|---|---|
| $Mg_2Si$ | Bi | $n$ | 1.1 | 0.86 | 862 | -250 | 5.6 | 3.5 | 50 |
| $Mg_2Si$ | Sb | $n$ | 2.4 | 0.62 | 823 | -180 | 6.0 | 2.7 | 80 |
| $Mg_2Ge$ | Sb, Mg | $n$ | 4.6 | 0.20 | 740 | -128 | 11.9 | 6.9 | 28 |
| $Mg_2Si_{0.5}Sn_{0.5}$ | Bi | $n$ | n.a. | 0.78 | 800 | -252 | 2.3 | 1.5 | 81 |
| $Mg_2Si_{0.4}Sn_{0.6}$ | Sb, Mg | $n$ | 8.0 | 0.85 | 700 | -217 | 6.0 | 2.3 | 82 |
| $Mg_2Si_{0.55}Sn_{0.4}Ge_{0.05}$ | Bi | $n$ | 2.2 | 1.40 | 800 | -219 | 7.3 | 2.0 | 83 |
| $Mg_2Si_{0.3}Sn_{0.7}$ | Li | $p$ | 4.9 | 0.50 | 750 | 161 | 6.2 | 2.5 | 43 |
| $Mg_2Si_{0.6}Ge_{0.4}$ | Ga | $p$ | 0.3 | 0.36 | 625 | 350 | 8.0 | 1.8 | 55 |

 This journal is © The Royal Society of Chemistry 2017

Please do not adjust margins

Please do not adjust margins



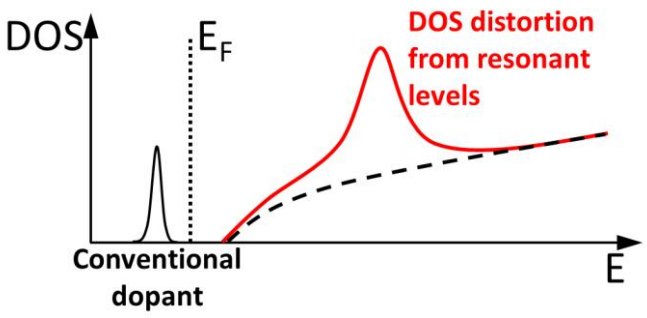


Figure 7. Schematic representation of the effect of a conventional *n*-type dopant and of a resonant level on the conduction band. Adapted from[90].

## 4. Magnesium non-stoichiometry

Synthesizing magnesium-based materials has inherent challenges related to its high volatility, eventually resulting in non-stoichiometric compositions of the final compounds, which, even when on a small scale, have a significant effect on the electrical properties of these materials. In general, excess Mg atoms occupy interstitial sites and donate two electrons to the conduction band[82], while in the case of Mg deficiency, each vacancy acts as a double hole donor[92, 93].

Works on Sb-doped $Mg_2Ge$ synthesized through different techniques have demonstrated the impact of excess and deficient Mg[28, 94-96] on the electron concentration and ultimately, the thermoelectric properties: despite all of them having been doped with similar concentrations of Sb, the compositions with excess Mg exhibited electron concentrations of ~6 × $10^{20}$ $cm^{-3}$ while ~2 × $10^{18}$ $cm^{-3}$ was reported for the Mg deficient ones. A more thorough study on the effects of Mg interstitials in $Mg_{2(1+x)}Si_{0.38}Sn_{0.6}Sb_{0.02}$ ($0.05 \leq x \leq 0.12$)[82] showed that their contribution to the carrier concentration can even supplant that of the dopant, which can be detrimental when precise control of the carrier concentration is needed.

### 4.1 Synthesis methods

As discussed previously, the stoichiometry of magnesium is likely to be the most important factor contributing to the thermoelectric properties of this class of thermoelectric materials. Typically, around 2-10 at.% excess Mg is added to the stoichiometric composition[60, 97-99], as its high vapor pressure and reactivity lead to significant losses by evaporation and the formation of other compounds such as MgO due to its strong affinity for oxygen[100]. Oxides are electrically insulating, and they are therefore undesirable within the bulk material and at the contact interfaces. As the formation of some MgO is practically certain, efforts are concentrated on reducing its formation, by handling and reacting high purity materials in oxygen-free atmosphere. Further losses of Mg through evaporation or reaction with crucibles are common at high temperature, which also need to be addressed.

Synthesizing thermoelectric materials is rarely seen as simply transforming raw materials into the desired thermoelectric compound. The type of starting materials – powders, pellets, etc. –, the temperature and duration of reactions, the cooling rate, and homogenization steps are all synthesis variables often used to affect the structural characteristics of materials, with significant impact on the thermoelectric properties, as detailed previously.

Fabricating magnesium-based compounds can be done using traditional methods such as reaction melting and solid-state synthesis, although particular challenges related to reacting Mg must be taken into consideration. With temperature as a promoter of Mg loss, either through evaporation or reaction, researchers looked at low temperature synthesis methods. Mechanical alloying methods such as planetary ball milling have been reported for the synthesis of $Mg_2Si$ using alumina vial and balls, and stainless steel vial and balls[101], although the authors reported that, even after 30 hours of milling, complete reaction was still not still achieved, and there was significant contamination by the grinding tools. Magnesium does not fracture easily due to its high ductility, aggregating when subjected to mechanical stress, delaying or even preventing reactions from occurring. This problem can be addressed by restricting the amount of available Mg that can aggregate through incremental additions to the ball-milling vial[68], greatly reducing the milling time required. Mechanical alloying reduces the Mg losses to practically zero, due to it being conducted at low temperature and in Ar atmosphere[53]. This process is often used as a mixing and homogenization step, before reaction through other methods[56, 95, 99]. Other synthesis processes have focused on the reduction of high temperature steps and/or their duration: $Mg_2Si$[102], $Mg_2Ge$[95], and $Mg_2Si_{0.6}Sn_{0.4}$[103] have been synthesized through a one-step SPS method, which utilizes the instant reaction of Si/Ge with the Mg precursor $MgH_2$, after temperature-driven $H_2$ liberation. Magnesium-based thermoelectric materials are more commonly fabricated through a solid-state synthesis method, which relies on the reaction of elements at temperatures below their melting point. $Mg_{2.16}(Si_{0.3}Sn_{0.7})_{0.98}Sb_{0.2}$ was fabricated using a two-step solid-state reaction method, at 873 K for 24 h and 1080 K for 24 h, where high purity powders were loaded into boron nitride crucibles and sealed in $SiO_2$ ampoules[40]. The reaction using this method is usually assisted by cold-pressing the starting materials into a compact disc, promoting diffusion when heated[43, 78, 104, 105]. Single-step solid-state reactions [75, 106, 107] and complete melting of the starting materials[25, 108, 109] are also commonly reported. The highly reactive nature of Mg at high temperature, such as with $SiO_2$, provides another challenge for the reaction of these materials, leading to investigations on the use of reaction crucibles, such as from molybdenum foil[73], tantalum[110], alumina sealed by $B_2O_3$[111], boron nitride[32], and graphite[60]. Magnesium-based thermoelectric materials are also reported to have been synthesized through less common techniques such as melt spinning[112], where the molten materials are injected onto a



Please do not adjust margins

Please do not adjust margins



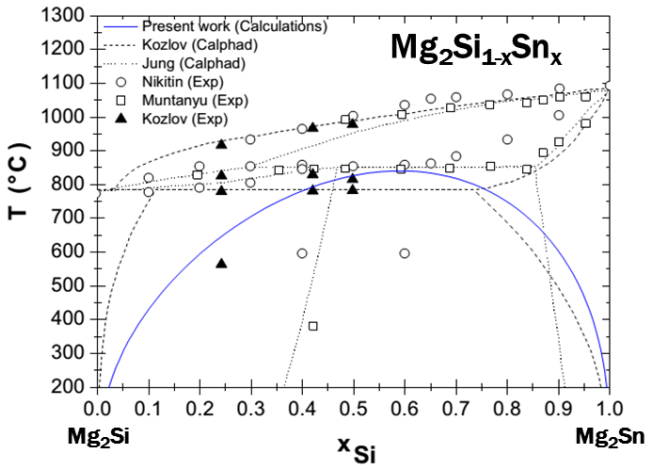


Figure 8. Calculated phase diagram and comparable data from the literature on the $Mg_2Si$-$Mg_2Sn$ quasi-binary phase diagram[115].

rotating chilled copper roller, quickly solidifying in the form of thin ribbons. Independently of the reaction method used, the fabrication of these materials is normally complemented by a densification step such as hot pressing[24, 99, 104] or spark plasma sintering[64, 108, 112]. The latter greatly reduces the duration of this step by promoting the sintering of particles through passage of an electrical current when pressure is applied, allowing for certain nanostructures to be maintained. Hot pressing, on the other hand, relies on the heating of powders through conduction of heat for extended periods of time at high temperature, usually inducing grain growth and homogenization of phases and structures within the material.

## 5. Solid solutions and phase diagrams

Despite the considerable volume of work on Mg-based thermoelectric materials, little is known about their stability at high operating temperatures. Most authors limit their research to supposedly single-phase, precipitate-free compositions as they are expected to exhibit higher performance and thermodynamic stability. Furthermore, there is no consensus on which compositions are single-phase, and most studies have focused on the significant enhancement of various properties through alloying[59, 60]. Early work on the $Mg_2Si$-$Mg_2Sn$ system focused on the optimization of the carrier concentration of $x \sim 0.4$ and $x \sim 0.6$ $Mg_2Si_{1-x}Sn_x$ compounds, considering these as the limits of the miscibility gap for these alloys[42]. Subsequent reports on these compounds use this study as their main reference when discussing the solid solution limit of $Mg_2Si_{1-x}Sn_x$. Study of the miscibility or solid solution gap of $Mg_2X$ ($X$ = Si, Ge, Sn) compounds has received relatively little attention, considering its importance for the stability of these materials when they are subject to high operating temperature and thermal cycling. There are, however, experimental and theoretical studies addressing this issue, along with reports on the solid solution stability range[42, 61, 113-116]. For instance, ab-initio calculations were used to theoretically investigate the phase stability of $Mg_2Si_{1-x}Sn_x$ and compare them with other theoretical and experimental thermodynamic reports[115] on the same compound (Figure 8). These suggest that the miscibility gap is wider than what has been previously accepted, and the author concludes that reports on high $zT$ thermoelectrics are likely not single-phase, questioning the stability of their thermoelectric properties in high temperature applications over an extended time. The discrepancy between reports on single-phase compounds and ab-initio phase stability calculations[115] has been reinforced in recent works on $Mg_2Si$-$Mg_2Sn$ thermoelectric materials, where electron microscopy techniques were used to observe more than one phase in these compounds, which could not be completely resolved by X-ray analysis[60, 104].

Table 5. Reported miscibility gaps and corresponding synthesis methods for $Mg_2Si_{1-x}Sn_x$ [113].

| Synthesis method | Miscibility gap, $x$ | Ref. |
|---|---|---|
| Flux method | 0.2-0.45 | 113 |
| Melting | 0.4-0.6 | 117, 118 |
| Liquid-solid reaction and hot pressing | No gap | 119 |
| Mechanical alloying and hot uniaxial pressing | 0.09-0.72 | 114 |
| Synthesis in sealed corundum crucible | 0.08-0.65 | 120 |
| Calculated | 0.08-0.66 | 116 |

The variation in the reported miscibility gap of $Mg_2Si_{1-x}Sn_x$ is considered to be a result of the kinetics of the formation of Sn- or Si-rich phases[116], suggesting a relationship with the synthesis method. Phase diagrams represent the existence of limits and transformations of compounds in thermodynamic equilibrium, and cannot be accurately used to predict the outcomes of most commonly used fabrication techniques. A systematic study of the structure of $Mg_2Si_{1-x}Sn_x$ for $0.1 \leq x \leq 0.8$, which was synthesized using a $B_2O_3$ flux method[113], reported significantly different miscibility gaps from those in the literature and compiled a list correlating the different results with the synthesis method used (Table 5). The authors point out the wide variability of reported miscibility gaps and suggest dependence on the final Mg stoichiometry obtained with each synthesis method.

## 6. Applications and devices

The functional unit of a thermoelectric device, generator, or cooling/heating system, is the thermoelectric couple or pair. A thermoelectric pair consists of $n$-type and $p$-type semiconducting materials connected electrically in series through metallic contacts and thermally in parallel, using electrically insulating but thermally conductive ceramic plates, in such a way that a temperature differential is allowed

 This journal is © The Royal Society of Chemistry 2017

Please do not adjust margins

Please do not adjust margins



through the length of the pair (Figure 9)[15]. Connecting several of these pairs creates a thermoelectric module or Peltier device.

When under operation, these devices are subjected to very large mechanical stress, even in the absence of vibration, due to thermal cycling and high temperature gradients. The effects of high temperature on the properties of these materials are also of great concern, particularly due to the fact that two distinct semiconducting materials are being used, raising the issue of compatibility with each other and with the electrical contacts due to diffusion of elements and chemical reactions at interfaces, often demanding the use of intermediate layers acting as diffusion barriers. Maintaining electrical contact between the thermoelectric legs and the electrical contacts presents another challenge, as simple solutions such as solders are not feasible at high temperatures, often requiring the direct bonding of the electrodes and the semiconductor.[15, 121]

The operational conditions for medium-to-high temperature thermoelectrics impose strict constraints on the selection of compatible materials for the assembly of a device. The simplest method when approaching these compatibility challenges is to use the same base thermoelectric material for both *n*- and *p*-type legs, reducing thermal expansion coefficient discrepancies between the two and possibly decreasing the complexity of the choice of electrode material. It is uncommon, however, for thermoelectric materials to exhibit high *zT* for both *n*- and *p*-type materials: as shown in Figure 3. For example, *n*-type $Mg_2Si_{0.3}Ge_{0.05}Sn_{0.65}$ boasts a *zT* at ~750 K of 1.4 while *p*-type $Mg_2Ge_{0.4}Sn_{0.6}$ only reaches a maximum *zT* of 0.5 at around the same temperature. Despite the low efficiency of *p*-type Mg-based thermoelectric materials, some preliminary results on device design and construction of devices based on these materials has already been achieved[15, 16, 58, 121-124]. The low performance of the *p*-type Mg-based thermoelectric materials creates serious limitations on the construction of devices, and most reports on the use of these materials in modules are on *n*-type legs[15, 58, 121]. Modules pairing *n*-type $Mg_2(Si_{0.4}Sn_{0.6})_{0.99}Sb_{0.01}$ and $Mg_2Si_{0.53}Sn_{0.4}Ge_{0.05}Bi_{0.02}$ with *p*-type $MnSi_{1.75}Ge_{0.01}$ were reported to reach a maximum power output of 3.24 W at 735 °C, achieving an estimated efficiency of 5.3%[122]. The authors report significant oxidation and decomposition of the hot side of the *n*-type leg, however, and they suggest that oxidation-preventing coatings could resolve this issue and that the development of effective diffusion layers and better bonding methods is needed.

Despite the significant challenges ahead for research on Mg-based thermoelectric devices, interest in these materials is not expected to fade. The highest *zT* composition of this family of materials, $Mg_2Si_{0.6}Sn_{0.4}$, is reported to have a material cost of $4/kg, significantly cheaper than the currently commercialized materials such as $Bi_2Te_3$, PbTe, and SiGe, with material costs of $110/kg, $81/kg, and $371/kg, respectively[125]. Table 6 compares state-of-art thermoelectric devices containing magnesium-based materials and other thermoelectric materials.

There are at least two companies utilizing magnesium-based thermoelectric materials in commercially available products: Alphabet Energy, which produces modules and generators using an *n*-type $Mg_2Si$-$Mg_2Sn$ compound paired with a *p*-type Cu-Sb-S compound, known as tetrahedrite, both thermoelectric systems that are recognized for their relatively good performance at medium-to-high temperatures and low price[126]; and Romny Scientific, which commercializes materials and modules fabricated using both *n*- and *p*-type $Mg_2Si$-$Mg_2Sn$[127].

### 6.1 Electrode bonding materials

Reports on thermoelectric generators using magnesium-based materials are still limited to $Mg_2Si$ as the *n*-type leg, and therefore, development of bonding techniques and electrode materials are also in their preliminary stages. Bi-doped $Mg_2Si$ has been used as the hot-side *n*-type thermoelectric material in a segmented leg[132], where $Bi_2Te_3$ is first bonded to $Mg_2Si$ by evaporating 50 nm of Ti and 1 μm of Ag on both surfaces before using Ag solder. Ti is expected to increase the adhesion between the semiconductors and Ag acts as "glue" due its low wetting angle. Then, Cu electrode was brazed to the $Mg_2Si$ using an Ag-Cu-Sn-Zn alloy. The cold side was bonded to the Cu electrode using a common Pb solder, because no significant reaction is expected to occur at low temperature. The total resistance of the electrodes, segmented legs, and respective bonding interfaces is reported to represent less than 2% (50 $\mu\Omega cm^2$) of the internal resistance of the materials used. $Mg_2Si$ is normally bonded to Ni[16, 123, 133] because at its working temperature, these materials are not expected to react[16, 133]. Ni has been directly bonded by SPS to Sb-doped $Mg_2Si$ powder between two layers of Ni powder[133], with its thermoelectric

Table 6. State-of-the-art thermoelectric devices. $T_h$ and $T_c$ are the temperatures of the hot-side and the cold side of the devices, respectively, and $\eta$ is the thermoelectric conversion efficiency. Materials separated with "+" are segmented legs. (Structure: *n*-type/*p*-type).

| Materials | $T_h/T_c$ (°C) | $\eta$ (%) | Ref. |
|---|---|---|---|
| $Mg_2Si_{0.53}Sn_{0.4}Ge_{0.05}/MnSi_{1.75}Ge_{0.01}$ | 735/50 | 5.3 | 122 |
| $Bi_{0.4}Sb_{1.6}Te_3$ + $CeFe_{3.85}Mn_{0.15}Sb_{12}$/ $Bi_2Te_{2.5}Se_{2.5}$ + $Yb_{0.3}Co_4Sb_{12}$ | 576/35 | 12.0 | 128 |
| $Bi_2Te_3$ + PbTe/$Bi_2Te_3$ + PbTe-MgTe | 600/30 | 11.0 | 129 |
| Unileg *p*-$MgAg_{0.965}Ni_{0.005}Sb_{0.99}$ | 250/25 | 8.5 | 130 |
| $Yb_{0.35}Co_4Sb_{12}/NdFe_{3.5}Co_{0.5}Sb_{12}$ | 550/70 | 9.1 | 131 |

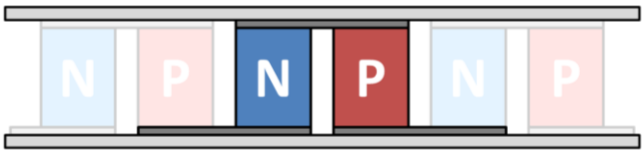


Figure 9. Schematic diagram of a thermoelectric module, with a pair highlighted. The pairs are connected electrically in series through metallic contacts (dark grey) and thermally in parallel through ceramic plates (light grey). This configuration allows for the maintenance of a temperature differential from one ceramic plate to the other through the thermoelectric material.



Please do not adjust margins

Please do not adjust margins



legs representing 12% (29.9 mΩcm$^2$) of the total resistance. SPS was also used for bonding bulk Cu and Ni foil to $Mg_2Si$ during the reaction of Mg and Si powders, forming a Cu/Ni/$Mg_2Si$/Ni/Cu structure[123]. In this study, the authors performed a more in-depth analysis of the Ni/$Mg_2Si$ interfaces and reported the formation of Ni-Si phases (Figure 10), obtaining a contact resistance of 1.44 mΩ·cm$^2$. The bonding of Ni foil to pre-reacted $Mg_2Si$ powder by SPS[16] led to an interface consisting of ternary phase Mg-Si-Ni and Si-Ni, resulting in high adhesion and very low contact resistance of 4.4 μΩcm$^2$. The synthesis of $Mg_2Si$ and bonding with Ni in a single step consistently result in lower contact resistance due to the perfectly intimate contact between the two materials the through formation of intermediate phases. This intimate contact is not possible when Ni is bonded to bulk (already formed) $Mg_2Si$, resulting in contact resistance around an order of magnitude higher[124, 134]. Ti, $TiSi_2$, and TiN were studied as candidate materials for diffusion barrier layers between Ni contacts and thermoelectric $Mg_2Si$, as these react at high temperature and form resistive phases[135]. Deposited TiN has shown particularly promising results by preventing significant diffusion of Mg while maintaining low contact resistance after annealing. Bonding of Mo electrodes was also reported on the hot side of high $zT$ $Mg_2(Si_{0.4}Sn_{0.6})_{0.99}Sb_{0.01}$ and $Mg_2Si_{0.53}Sn_{0.4}Ge_{0.05}Bi_{0.01}$, after deposition of thin layers of Ni, Pb, and Cr to improve contact and adhesion[122]. At this point in the development of magnesium-based thermoelectric devices, research efforts are still focused on the development and optimization of bonding techniques and materials, although the long-term stability and impact of the materials used for the junctions on the thermoelectric and mechanical properties of the device are critical to the technology and are yet to be explored.

## 7. Summary and outlook

In this work, we have reviewed the general position occupied by magnesium-based thermoelectric materials in terms of performance, challenges, and advantages, in relation to other thermoelectric materials. This group of thermoelectric materials has been garnering considerable interest due to the high $zT$ values obtained in its *n*-type materials at medium-to-high temperatures, while it is considered to be low-cost with high availability, non-toxicity, and very low density. $Mg_2X$ ($X$ = Si, Ge, Sn) binary and ternary alloys provide a wide range of compositions to explore, with many performance-enhancing pathways available, such as band engineering, by inducing band convergence[42, 49] and/or resonant states[91]; complete dissolution of elements, providing stable solid solutions[58, 59], or phonon-scattering features in intermetallic compositions[24, 60, 62], as well as the possibility of building thermoelectric modules using both *n*- and *p*-type magnesium-based materials, greatly reducing compatibility issues[15]. Recent studies have been focused on understanding the mechanisms responsible for the current performance of magnesium-based materials, although an application-driven research approach may be necessary to solve challenges such as doping optimization – particularly for *p*-type compounds, long term and high temperature compositional and structural stability, the development of synthesis processes that provide precise control of the final stoichiometry, thermomechanical studies on the reliability of these systems under adverse conditions while in operation, and the bonding of compatible electrical contacts. Despite being mostly seen as potential alternatives to the higher efficiency materials, such as PbTe[29], magnesium-based thermoelectric compounds exhibit exciting techno-economic characteristics that are relevant when considering viable thermoelectric materials for large-scale applications, particularly the aforementioned low mass density and low cost of the raw materials. Therefore, the development of high efficiency *p*-type magnesium-based compounds could be the breakthrough required for worldwide application of these materials. The particular challenges related to *p*-type optimization center mostly around the low charge carrier density achieved in these materials, aggravated by the limited number of compatible dopants, comprising Ag, Li, and Ga, with Li being the most promising dopant. A double-doping approach with combinations of these three elements might be the key to achieving high charge carrier concentrations in *p*-type magnesium-based thermoelectric materials. Most synthesis methods further contribute to a low charge carrier density, as excess magnesium in the final compounds occupies interstitial positions in the lattice and acts as an electron donor. Beyond their overall negative impact on the power factor, low doping densities generally lead to the manifestation of the bipolar effect at lower temperatures, which effectively decreases their maximum operating temperature. Reports on the variable solubility of dopants in the Mg-based binary phases depending on the fabrication method open the door to exploring new ways of increasing hole concentrations. The inconsistency concerning the solubility limits of dopants and solid solution ranges in these materials usher in exciting opportunities to explore. Concepts such as selective doping of secondary phases within a matrix, known as modulated doping – in the form of phonon disruptive structures such as nanodots, grain-surrounding nanolayers, or compositionally modulated structures[136, 137], with dopant elements having temperature dependent solubility, are techniques yet to be studied for this class of thermoelectric materials. Non-equilibrium techniques are often required in the development of these structures, but their benefits are undermined by low long-term thermal stability.

As the synthesis of magnesium-based thermoelectric materials is still under development, work on their application in thermoelectric devices is still in its infancy. Less attention has been devoted to the long-term stability of these compounds at high temperature, in terms of either thermoelectric or mechanical properties. Such studies are essential to ensure their future applicability. Consequently, reports on the bonding of electrical contacts are also still lacking, as this work offers significant engineering challenges by requiring high adhesion between the materials while maintaining their

 This journal is © The Royal Society of Chemistry 2017

Please do not adjust margins

Please do not adjust margins



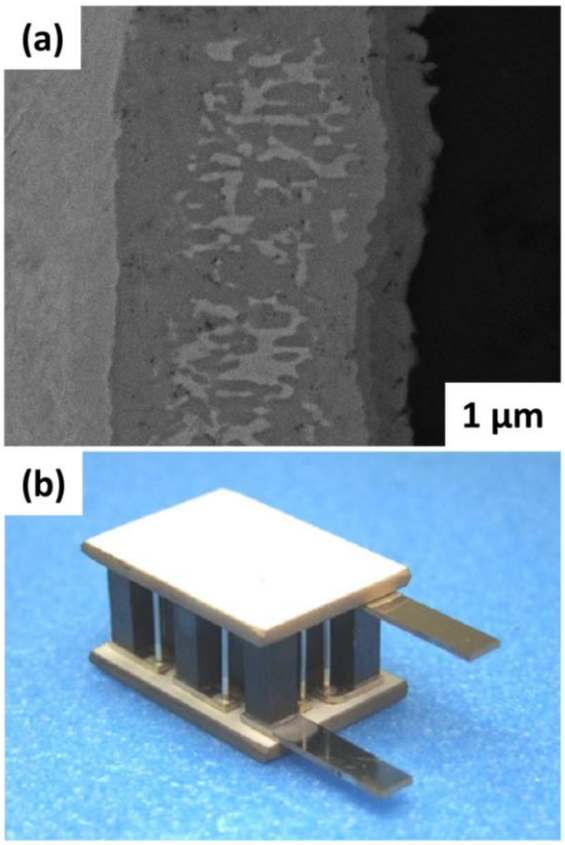


Figure 10. (a) Secondary electron image of a Ni/$Mg_2Si$ interface after sintering for 15 min at 1023 K[123], showing pure Ni as a bright phase on the left, $Mg_6Si_7Ni_{16}$ phase in dark grey with precipitates of $Ni_2Si$ in light grey, followed by $(Mg_{0.52}Ni_{0.48})_7Si_4$[138] in darker grey and $Mg_2Si$ in black. (b) Unileg device, consisting of ten thermoelectric legs of Sb-doped $Mg_2Si$ legs[133].

mechanical and thermoelectric characteristics at high temperature.

Despite the great number of challenges ahead for developing magnesium-based thermoelectric devices, their promising potential advantages make them very interesting, particularly from an commercial point-of-view, and they are sure to arouse further interest as their development approaches real-world device suitability.

## Conflicts of interest

There are no conflicts to declare.

## Acknowledgements

We would like to thank the Australian Research Council (ARC) for financial support provided via a Linkage Project grant (LP120200289) and an ARC Discovery Early Career Award (DE130100310).

## Notes and references

1 U.S. Department of Energy, *Lawrence Livermore National Laboratory*, 2017.
2 J. He, M. G. Kanatzidis and V. P. Dravid, *Materials Today*, 2013, **16**, 166-176.
3 H. A. Gabbar, C. A. Barry Stoute, D. Steele, C. Simkin, T. Sleeman, D. Newell, D. Paterson and E. Boafo, *Annals of Nuclear Energy*, 2017, **101**, 454-464.
4 K. Yazawa, M. Hao, B. Wu, A. K. Silaen, C. Q. Zhou, T. S. Fisher and A. Shakouri, *Energy Conversion and Management*, 2014, **84**, 244-252.
5 B. Orr, A. Akbarzadeh, M. Mochizuki and R. Singh, *Applied Thermal Engineering*, 2015.
6 S. Yu, Q. Du, H. Diao, G. Shu and K. Jiao, *Applied Energy*, 2015, **138**, 276-290.
7 T. Kuroki, R. Murai, K. Makino, K. Nagano, T. Kajihara, H. Kaibe, H. Hachiuma and H. Matsuno, *Journal of Electronic Materials*, 2015, **44**, 2151-2156.
8 H. Zhang, L. Dong, H.-q. Li, B. Chen, Q. Tang and T. Fujita, *Sustainable Energy Technologies and Assessments*, 2013, **2**, 67-80.
9 G. J. Snyder and E. S. Toberer, *Nature Materials*, 2008, **7**, 105-114.
10 S. N. Guin, A. Chatterjee, D. S. Negi, R. Datta and K. Biswas, *Energy & Environmental Science*, 2013, **6**, 2603.
11 D. Champier, *Energy Conversion and Management*, 2017, **140**, 167-181.
12 A. Banik and K. Biswas, *Journal of Materials Chemistry A*, 2014, **2**, 9620.
13 S. LeBlanc, *Sustainable Materials and Technologies*, 2014, **1-2**, 26-35.
14 Y. Pei, H. Wang and G. J. Snyder, *Adv Mater*, 2012, **24**, 6125-6135.
15 D. M. Rowe, *Thermoelectrics Handbook: Macro to Nano*, CRC Press, Taylor & Francis Group, Boca Raton, FL, 1st edn., 2006.
16 J. de Boor, C. Gloanec, H. Kolb, R. Sottong, P. Ziolkowski and E. Müller, *Journal of Alloys and Compounds*, 2015, **632**, 348-353.
17 K. Koumoto and T. Mori, *Thermoelectric Nanomaterials: Materials Design and Applications*, Springer Science & Business Media, 2013.
18 Y. I. Ravich, B. A. Efimova and I. A. Smirnov, *Semiconducting Lead Chalcogenides*, Springer, 1970.
19 C. M. Bhandari, in *CRC Handbook of Thermoelectrics*, ed. D. M. Rowe, CRC Press, 1995.
20 M. G. Kanatzidis, *Chemistry of Materials*, 2010, **22**, 648-659.
21 G. Bernard-Granger, R. Vracar, C. Navone, J. Leforestier, M. Boidot, J. Carrete, B. Deniau and J. Simon, *Scripta Materialia*, 2015, **104**, 5-8.
22 H. Y. Chen, N. Savvides, T. Dasgupta, C. Stiewe and E. Mueller, *physica status solidi (a)*, 2010, **207**, 2523-2531.
23 S. Wang and N. Mingo, *Applied Physics Letters*, 2009, **94**, 203109.
24 N. Farahi, S. Prabhudev, M. Bugnet, G. A. Botton, J. R. Salvador and H. Kleinke, *Journal of Electronic Materials*, 2016, **45**, 6052-6058.
25 H. Ning, G. D. Mastrorillo, S. Grasso, B. Du, T. Mori, C. Hu, Y. Xu, K. Simpson, G. Maizza and M. J. Reece, *J. Mater. Chem. A*, 2015, **3**, 17426-17432.
26 S. Perumal, S. Gorsse, U. Ail, B. Chevalier, R. Decourt and A. M. Umarji, *Journal of Materials Science*, 2012, **48**, 227-231.
27 C. E. Kim, A. Soon and C. Stampfl, *Physical Chemistry Chemical Physics*, 2016, **18**, 939-946.
28 H. L. Gao, T. J. Zhu, X. B. Zhao and Y. Deng, *Intermetallics*, 2015, **56**, 33-36.
29 Z. L. Du, H. L. Gao and J. L. Cui, *Current Applied Physics*, 2015, **15**, 784-788.



Please do not adjust margins

Please do not adjust margins




30 V. K. Zaitsev, M. I. Fedorov, E. A. Gurieva, I. S. Eremin, P. P. Konstantinov, A. Yu. Samunin and M. V. Vedernikov, *International Conference on Thermoelectrics*, 2005.
31 T. Aizawa, R. Song and A. Yamamoto, *Materials Transactions*, 2005, **46**, 1490-1496.
32 K. Yin, X. Su, Y. Yan, Y. You, Q. Zhang, C. Uher, M. G. Kanatzidis and X. Tang, *Chemistry of Materials*, 2016, **28**, 5538-5548.
33 S. I. Kim, K. H. Lee, H. A. Mun, H. S. Kim, S. W. Hwang, J. W. Roh, D. J. Yang, W. H. Shin, X. S. Li, Y. H. Lee, G. J. Snyder and S. W. Kim, *Science*, 2015, **348**, 109-114.
34 D. Wu, L.-D. Zhao, X. Tong, W. Li, L. Wu, Q. Tan, Y. Pei, L. Huang, J.-F. Li, Y. Zhu, M. G. Kanatzidis and J. He, *Energy & Environmental Science*, 2015, **8**, 2056-2068.
35 Q. Zhang, X. Li, Y. Kang, L. Zhang, D. Yu, J. He, Z. Liu, Y. Tian and B. Xu, *Journal of Materials Science: Materials in Electronics*, 2014, **26**, 385-391.
36 Y. Gelbstein, J. Davidow, S. N. Girard, D. Y. Chung and M. Kanatzidis, *Advanced Energy Materials*, 2013, **3**, 815-820.
37 S. Bathula, M. Jayasimhadri, N. Singh, A. K. Srivastava, J. Pulikkotil, A. Dhar and R. C. Budhani, *Applied Physics Letters*, 2012, **101**, 213902.
38 R. Morris, R. Redin and G. Danielson, *Physical Review*, 1958, **109**, 1909-1915.
39 M. W. Heller and G. C. Danielson, *J. Phys. Chem. Solids*, 1962, **23**, 601-610.
40 K. Yin, X. Su, Y. Yan, H. Tang, M. G. Kanatzidis, C. Uher and X. Tang, *Scripta Materialia*, 2017, **126**, 1-5.
41 V. K. Zaitsev, M. I. Fedorov, E. A. Gurieva, I. S. Eremin, P. P. Konstantinov, A. Y. Samunin and M. V. Vedernikov, *2005 International Conference on Thermoelectrics*, 2005, 7.
42 V. K. Zaitsev, M. I. Fedorov, E. A. Gurieva, I. S. Eremin, P. P. Konstantinov, A. Y. Samunin and M. V. Vedernikov, *Physical Review B*, 2006, **74**, 045207.
43 Q. Zhang, L. Cheng, W. Liu, Y. Zheng, X. Su, H. Chi, H. Liu, Y. Yan, X. Tang and C. Uher, *Physical Chemistry Chemical Physics*, 2014, **16**, 23576-23583.
44 X. Shi, L. Chen and C. Uher, *International Materials Reviews*, 2016, **61**, 379-415.
45 P. Gao, I. Berkun, R. D. Schmidt, M. F. Luzenski, X. Lu, P. Bordon Sarac, E. D. Case and T. P. Hogan, *Journal of Electronic Materials*, 2013, **43**, 1790-1803.
46 S. Ganeshan, S. L. Shang, Y. Wang and Z. K. Liu, *Journal of Alloys and Compounds*, 2010, **498**, 191-198.
47 K. Kutorasinski, B. Wiendlocha, J. Tobola and S. Kaprzyk, *Physical Review B*, 2014, **89**, 8.
48 P. Boulet, M. J. Verstraete, J. P. Crocombette, M. Briki and M. C. Record, *Computational Materials Science*, 2011, **50**, 847-851.
49 W. Liu, X. Tan, K. Yin, H. Liu, X. Tang, J. Shi, Q. Zhang and C. Uher, *Physical Review Letters*, 2012, **108**.
50 J.-i. Tani and H. Kido, *Physica B: Condensed Matter*, 2005, **364**, 218-224.
51 K. Mars, H. Ihou-Mouko, G. Pont, J. Tobola and H. Scherrer, *Journal of Electronic Materials*, 2009, **38**, 1360-1364.
52 Q. Zhang, H. Yin, X. B. Zhao, J. He, X. H. Ji, T. J. Zhu and T. M. Tritt, *phys. stat. sol. (a)*, 2008, **205**, 1657-1661.
53 W. Liu, H. S. Kim, S. Chen, Q. Jie, B. Lv, M. Yao, Z. Ren, C. P. Opeil, S. Wilson, C. W. Chu and Z. Ren, *Proc Natl Acad Sci U S A*, 2015, **112**, 3269-3274.
54 T.-H. An, C. Park, W.-S. Seo, S.-M. Choi, I.-H. Kim and S.-U. Kim, *Journal of the Korean Physical Society*, 2012, **60**, 1717-1723.
55 H. Ihou-Mouko, C. Mercier, J. Tobola, G. Pont and H. Scherrer, *Journal of Alloys and Compounds*, 2011, **509**, 6503-6508.
56 J. de Boor, U. Saparamadu, J. Mao, K. Dahal, E. Müller and Z. Ren, *Acta Materialia*, 2016, **120**, 273-280.
57 X. Wang and Z. M. Wang, *Nanoscale Thermoelectrics*, Springer, 2014.
58 H. J. Goldsmid, *Introduction to Thermoelectricity*, Springer, 2nd edn., 2016.
59 V. K. Zaitsev, M. I. Fedorov, I. S. Eremin and E. A. Gurieva, in *Thermoelectrics Handbook: Macro to Nano*, ed. D. Rowe, Taylor & Francis, 2006.
60 N. Vlachos, E. Hatzikraniotis, C. N. Mihailescu, J. Giapintzakis and T. Kyratsi, *Journal of Electronic Materials*, 2014, **43**, 3844-3851.
61 Y. Isoda, T. Nagai, H. Fujui, Y. Imai and Y. Shinohara, *2007 International Conference on Thermoelectrics*, 2008, 251-255.
62 Q. Zhang, J. He, T. J. Zhu, S. N. Zhang, X. B. Zhao and T. M. Tritt, *Applied Physics Letters*, 2008, **93**, 102109.
63 Q. Zhang, J. He, X. B. Zhao, S. N. Zhang, T. J. Zhu, H. Yin and T. M. Tritt, *Journal of Physics D: Applied Physics*, 2008, **41**, 185103.
64 L. Zheng, X. Zhang, H. Liu, S. Li, Z. Zhou, Q. Lu, J. Zhang and F. Zhang, *Journal of Alloys and Compounds*, 2016, **671**, 452-457.
65 V. K. Zaitsev, M. I. Fedorov, I. S. Eremin and E. A. Gurieva, in *Thermoelectrics Handbook: Macro to Nano*, ed. D. M. Rowe, CRC Press, Boca Raton, FL, USA, 2006, ch. 29.
66 N. Satyala and D. Vashaee, *Journal of Applied Physics*, 2012, **112**, 093716.
67 T. Ikeda, L. Haviez, Y. Li and G. J. Snyder, *Small*, 2012, **8**, 2350-2355.
68 S. K. Bux, M. T. Yeung, E. S. Toberer, G. J. Snyder, R. B. Kaner and J.-P. Fleurial, *Journal of Materials Chemistry*, 2011, **21**, 12259.
69 D. A. Pshenai-Severin, M. I. Fedorov and A. Y. Samunin, *Journal of Electronic Materials*, 2013, **42**, 1707-1710.
70 D. Cederkrantz, N. Farahi, K. A. Borup, B. B. Iversen, M. Nygren and A. E. C. Palmqvist, *Journal of Applied Physics*, 2012, **111**, 023701.
71 X. J. Tan, W. Liu, H. J. Liu, J. Shi, X. F. Tang and C. Uher, *Physical Review B*, 2012, **85**.
72 K. Kutorasinski, J. Tobola, S. Kaprzyk, A. U. Khan and T. Kyratsi, *Journal of Electronic Materials*, 2014, **43**, 3831-3837.
73 L. Zhang, P. Xiao, L. Shi, G. Henkelman, J. B. Goodenough and J. Zhou, *Journal of Applied Physics*, 2015, **117**, 155103.
74 H. Balout, P. Boulet and M. C. Record, *Intermetallics*, 2014, **50**, 8-13.
75 L. Zhang, P. Xiao, L. Shi, G. Henkelman, J. B. Goodenough and J. Zhou, *Journal of Applied Physics*, 2016, **119**, 085104.
76 K. Kutorasiński, J. Tobola and S. Kaprzyk, *Physical Review B*, 2013, **87**.
77 Y. Tang, Z. M. Gibbs, L. A. Agapito, G. Li, H. S. Kim, M. B. Nardelli, S. Curtarolo and G. J. Snyder, *Nature Materials*, 2015, **14**, 1223-1228.
78 Q. Zhang, Y. Zheng, X. Su, K. Yin, X. Tang and C. Uher, *Scripta Materialia*, 2015, **96**, 1-4.
79 S. O. Kasap, *Principles of Electronic Materials and Devices*, McGraw-Hill, 3rd edn., 2006.
80 J. Y. Jung, K. H. Park and I. H. Kim, *IOP Conference Series: Materials Science and Engineering*, 2011, **18**, 142006.
81 W. J. Luo, M. J. Yang, Q. Shen, H. Y. Jiang and L. M. Zhang, *Advanced Materials Research*, 2009, **66**, 33-36.
82 Z. Du, T. Zhu, Y. Chen, J. He, H. Gao, G. Jiang, T. M. Tritt and X. Zhao, *Journal of Materials Chemistry*, 2012, **22**, 6838.
83 A. U. Khan, N. V. Vlachos, E. Hatzikraniotis, G. S. Polymeris, C. B. Lioutas, E. C. Stefanaki, K. M. Paraskevopoulos, I. Giapintzakis and T. Kyratsi, *Acta Materialia*, 2014, **77**, 43-53.
84 J.-i. Tani and H. Kido, *Intermetallics*, 2008, **16**, 418-423.


 This journal is © The Royal Society of Chemistry 2017

Please do not adjust margins

Please do not adjust margins




85 J.-i. Tani, M. Takahashi and H. Kido, *Journal of Alloys and Compounds*, 2009, **485**, 764-768.
86 J.-i. Tani and H. Kido, *Physica B: Condensed Matter*, 2012, **407**, 3493-3498.
87 J.-i. Tani and H. Kido, *Intermetallics*, 2007, **15**, 1202-1207.
88 Y. Isoda, T. Nagai, H. Fujiu, Y. Imai and Y. Shinohara, *ICT '06. 25th International Conference on Thermoelectrics*, 2006, 406-410.
89 N. Satyala and D. Vashaee, *Journal of Electronic Materials*, 2012, **41**, 1785-1791.
90 J. P. Heremans, B. Wiendlocha and A. M. Chamoire, *Energy Environ. Sci.*, 2012, **5**, 5510-5530.
91 J. Bourgeois, J. Tobola, B. Wiendlocha, L. Chaput, P. Zwolenski, D. Berthebaud, F. Gascoin, Q. Recour and H. Scherrer, *Functional Materials Letters*, 2013, **06**, 1340005.
92 J. Tobola, S. Kaprzyk and H. Scherrer, *Journal of Electronic Materials*, 2009, **39**, 2064-2069.
93 A. Kato, T. Yagi and N. Fukusako, *Journal of Physics: Condensed Matter*, 2009, **21**, 205801.
94 G. S. Nolas, D. Wang and X. Lin, *physica status solidi (RRL) – Rapid Research Letters*, 2007, **1**, 223-225.
95 R. Santos, M. Nancarrow, S. X. Dou and S. A. Yamini, *Scientific Reports*, 2017, **7**, 3988.
96 R. Santos, S. X. Dou, D. Vashaee and S. A. Yamini, *ACS Omega*, 2017, **2**, 8069-8074.
97 W. Liu, H. Chi, H. Sun, Q. Zhang, K. Yin, X. Tang, Q. Zhang and C. Uher, *Physical Chemistry Chemical Physics*, 2014, **16**, 6893-6897.
98 W. Liu, Q. Zhang, X. Tang, H. Li and J. Sharp, *Journal of Electronic Materials*, 2011, **40**, 1062-1066.
99 J. Mao, H. S. Kim, J. Shuai, Z. Liu, R. He, U. Saparamadu, F. Tian, W. Liu and Z. Ren, *Acta Materialia*, 2016, **103**, 633-642.
100 E. Wiberg and N. Wiberg, *Inorganic Chemistry*, Academic Press, 2001.
101 X. Niu and L. Lu, *Advanced Performance Materials*, 1997, **3**, 275-283.
102 S. Chen, X. Zhang, W. Fan, T. Yi, D. V. Quach, S. Bux, Q. Meng, S. M. Kauzlarich and Z. A. Munir, *Journal of Alloys and Compounds*, 2015, **625**, 251-257.
103 W. Fan, S. Chen, B. Zeng, Q. Zhang, Q. Meng, W. Wang and Z. A. Munir, *ACS Appl Mater Interfaces*, 2017, **9**, 28635-28641.
104 G. S. Polymeris, N. Vlachos, A. U. Khan, E. Hatzikraniotis, C. B. Lioutas, A. Delimitis, E. Pavlidou, K. M. Paraskevopoulos and T. Kyratsi, *Acta Materialia*, 2015, **83**, 285-293.
105 S.-W. You, D.-K. Shin and I.-H. Kim, *Journal of the Korean Physical Society*, 2014, **64**, 1346-1350.
106 A. Kolezynski, P. Nieroda and K. T. Wojciechowski, *Computational Materials Science*, 2015, **100**, 84-88.
107 Y. Isoda, S. Tada, H. Kitagawa and Y. Shinohara, *Journal of Electronic Materials*, 2015, **45**, 1772-1778.
108 J.-W. Liu, M. Song, M. Takeguchi, N. Tsujii and Y. Isoda, *Journal of Electronic Materials*, 2015.
109 X. Hu, M. R. Barnett and A. Yamamoto, *Journal of Alloys and Compounds*, 2015, **649**, 1060-1065.
110 N. Farahi, S. Prabhudev, G. A. Botton, J. Zhao, J. S. Tse, Z. Liu, J. R. Salvador and H. Kleinke, *Journal of Alloys and Compounds*, 2015, **644**, 249-255.
111 H. Gao, T. Zhu, X. Liu, L. Chen and X. Zhao, *Journal of Materials Chemistry*, 2011, **21**, 5933.
112 X. Tang, Y. Zhang, Y. Zheng, K. Peng, T. Huang, X. Lu, G. Wang, S. Wang and X. Zhou, *Applied Thermal Engineering*, 2016.
113 L. Chen, G. Jiang, Y. Chen, Z. Du, X. Zhao, T. Zhu, J. He and T. M. Tritt, *Journal of Materials Research*, 2011, **26**, 3038-3043.
114 M. Riffel and J. Schilz, *15th International Conference on Thermoelectrics*, 1996, 133-136.
115 R. Viennois, C. Colinet, P. Jund and J.-C. Tédenac, *Intermetallics*, 2012, **31**, 145-151.
116 I.-H. Jung, D.-H. Kang, W.-J. Park, N. J. Kim and S. Ahn, *Calphad*, 2007, **31**, 192-200.
117 V. Zaitsev, M. Fedorov, E. Gurieva, I. Eremin, P. Konstantinov, A. Samunin and M. Vedernikov, *Physical Review B*, 2006, **74**.
118 E. Nikitin, E. Tkalenko, V. Zaitsev, A. Zaslavskii and A. Kuznetsov, *Inorg. Mater*, 1968, **4**, 1656.
119 Y. Isoda, T. Nagai, H. Fujiu, Y. Imai and Y. Shinohara, *2007 International Conference on Thermoelectrics*, 2008, 251-255.
120 A. Kozlov, J. Gröbner and R. Schmid-Fetzer, *Journal of Alloys and Compounds*, 2011, **509**, 3326-3337.
121 M. Zebarjadi, K. Esfarjani, M. S. Dresselhaus, Z. F. Ren and G. Chen, *Energy Environ. Sci.*, 2012, **5**, 5147-5162.
122 G. Skomedal, L. Holmgren, H. Middleton, I. S. Eremin, G. N. Isachenko, M. Jaegle, K. Tarantik, N. Vlachos, M. Manoli, T. Kyratsi, D. Berthebaud, N. Y. Dao Truong and F. Gascoin, *Energy Conversion and Management*, 2016, **110**, 13-21.
123 R. Yang, S. Chen, W. Fan, X. Gao, Y. Long, W. Wang and Z. A. Munir, *Journal of Alloys and Compounds*, 2017, **704**, 545-551.
124 S. Nakamura, Y. Mori and K. i. Takarabe, *Journal of Electronic Materials*, 2014, **43**, 2174-2178.
125 S. LeBlanc, S. K. Yee, M. L. Scullin, C. Dames and K. E. Goodson, *Renewable and Sustainable Energy Reviews*, 2014, **32**, 313-327.
126 A. Energy, Alphabet Energy Demonstrates Best-in-Class Thermoelectric Performance & Scalability with PowerCard™ Product, https://www.alphabetenergy.com/alphabet-energy-demonstrates-best-in-class-thermoelectric-performance-scalability-with-powercard-product/, (accessed October 20, 2017).
127 R. Scientific, Thermoelectric materials, http://romny-scientific.com/Products/quality-management/, (accessed 20 October 2017).
128 Q. Zhang, J. Liao, Y. Tang, M. Gu, C. Ming, P. Qiu, S. Bai, X. Shi, C. Uher and L. Chen, *Energy & Environmental Science*, 2017, **10**, 956-963.
129 X. Hu, P. Jood, M. Ohta, M. Kunii, K. Nagase, H. Nishiate, M. G. Kanatzidis and A. Yamamoto, *Energy & Environmental Science*, 2016, **9**, 517-529.
130 D. Kraemer, J. Sui, K. McEnaney, H. Zhao, Q. Jie, Z. F. Ren and G. Chen, *Energy & Environmental Science*, 2015, **8**, 1299-1308.
131 A. Muto, J. Yang, B. Poudel, Z. Ren and G. Chen, *Advanced Energy Materials*, 2013, **3**, 245-251.
132 H. S. Kim, K. Kikuchi, T. Itoh, T. Iida and M. Taya, *Materials Science and Engineering: B*, 2014, **185**, 45-52.
133 T. Nemoto, T. Iida, J. Sato, T. Sakamoto, N. Hirayama, T. Nakajima and Y. Takanashi, *Journal of Electronic Materials*, 2013, **42**, 2192-2197.
134 T. Sakamoto, T. Iida, Y. Honda, M. Tada, T. Sekiguchi, K. Nishio, Y. Kogo and Y. Takanashi, *Journal of Electronic Materials*, 2012, **41**, 1805-1810.
135 T. Sakamoto, Y. Taguchi, T. Kutsuwa, K. Ichimi, S. Kasatani and M. Inada, *Journal of Electronic Materials*, 2015, **45**, 1321-1327.
136 B. Yu, M. Zebarjadi, H. Wang, K. Lukas, H. Wang, D. Wang, C. Opeil, M. Dresselhaus, G. Chen and Z. Ren, *Nano Lett*, 2012, **12**, 2077-2082.
137 S. A. Yamini, D. R. G. Mitchell, Z. M. Gibbs, R. Santos, V. Patterson, S. Li, Y. Z. Pei, S. X. Dou and G. J. Snyder, *Advanced Energy Materials*, 2015, **5**, 1501047.




Please do not adjust margins

Please do not adjust margins



138 Y. K. Song and R. A. Varin, *Metallurgical and Materials Transactions A*, 2001, **32**, 5-18.

 This journal is © The Royal Society of Chemistry 2017

Please do not adjust margins